JACS
JOURNAL OF THE AMERICAN CHEMICAL SOCIETY

Communication

pubs.acs.org/JACS

MOFs Under Pressure: The Reversible Compression of a Single Crystal

Kevin J. Gagnon,*[,†] Christine M. Beavers,[‡] and Abraham Clearfield[†]

[†]Department of Chemistry, Texas A&M University, College Station, Texas 77840, United States

[‡]Advanced Light Source, Lawrence Berkeley National Laboratory, Berkeley, California 94720, United States

Supporting Information

ABSTRACT: The structural change and resilience of a single crystal of a metal−organic framework (MOF), $Zn(HO_3PC_4H_8PO_3H)\cdot 2H_2O$ (ZAG-4), was investigated under high pressures (0−9.9 GPa) using *in situ* single crystal X-ray diffraction. Although the unit cell volume decreases over 27%, the quality of the single crystal is retained and the unit cell parameters revert to their original values after pressure has been removed. This framework is considerably compressible with a bulk modulus calculated at ∼11.7 GPa. The *b*-axis also exhibits both positive and negative linear compressibility. Within the applied pressures investigated, there was no discernible failure or amorphization point for this compound. The alkyl chains in the structure provide a spring-like cushion to stabilize the compression of the system allowing for large distortions in the metal coordination environment, without destruction of the material. This intriguing observation only adds to the current speculation as to whether or not MOFs may find a role as a new class of piezofunctional solid-state materials for application as highly sensitive pressure sensors, shock absorbing materials, pressure switches, or smart body armor.

Metal−organic frameworks (MOFs) have revolutionized the field of crystal engineering, and stand to potentially revolutionize the field of solid-state chemistry.[1−5] The narrow definition of these materials is still under debate; however, the broad definition includes compounds exhibiting some level of dimensionality that are composed of metal-ions or cluster building units extended through coordinated organic linkers. Examples include carboxylates, phosphonates, and imidizoles to name a few.[6−8] Similar to any other class of solid-state materials, these new compounds exhibit a wide variety of unique chemical properties attractive for a diversity of applications from ion-exchange to gas storage/separations.[5] Now that these compounds have presented themselves as being useful for engineering applications, more information is needed as to the mechanical properties and limitations. This information will lead to a variety of beneficial applications including pressure switches, smart body armor, pressure sensors, or shock absorbing materials.

A recent review presented a number of cases where mechanical properties of hybrid materials had been investigated; however, that number was relatively small compared with the number of MOFs published to date.[9] Many of these cases were computational. Of the few experimental studies that have been conducted, very interesting properties have been uncovered. The study of crystalline compounds under hydrostatic pressure loading has yielded remarkable results.[9,10] One relevant find here has been on the role of hydrogen bonding in extended minerals. Parise and co-workers conducted a number of neutron scattering experiments on various hydrous minerals under pressure to show that the H−O bond lengths do not change; however, O···O distances do and the H atom positions may rearrange. One role they propose as being very relevant is that of the H···H repulsion. Chapman and co-workers have shown that the compressibility of crystalline MOFs can be affected by guest inclusion and that the porosity of these materials can be modified by treating them first with small pressures.[11,12] Moggach and co-workers have shown the effects of pressure on single crystalline porous frameworks, and the structural changes associated with forcing solvent into the pores.[13,14] The main application front for MOFs has been around gas storage and the understanding of how these structures change with applied pressure will be important if these materials are to have any industrial viability.

Even with the few pressure studies that have been conducted on MOFs, to the best of our knowledge, they have been conducted on rigid, highly porous or nonporous materials. The common factor between the examples is the rigidity of the linker. For a number of years, Clearfield and co-workers (among others) have routinely studied compounds formed utilizing alkyl chains as the linker molecules.[3,15] One of these materials was presented in a thesis from the Clearfield group[16] and later published by Fu and co-workers.[17] A recent review presented this compound and named it the zinc alkyl gate (ZAG), which when synthesized with 1,4-butanebis(phosphonic acid) is denoted as ZAG-4.[15] The name ZAG comes from the likeness of the structure, when viewed down the *c*-axis, to a collapsible pet or child safety gate (Figure 1). Herein, we investigate the effect of hydrostatic pressure (0 to ∼10 GPa) on the flexible framework ZAG-4. This framework was chosen as it is a chemically robust member of a family of related zinc-alkyl frameworks. ZAG-4 is comprised of Zn−O−P−O 8-membered rings fused through zinc into a 1-D chain which is hydrogen bonded in one direction to neighboring chains and cross-linked in the other direction by the butane linker. The hydrogen bonded channel is filled with two water molecules per formula unit.

The pressure dependent studies of ZAG-4 were conducted on a single crystal sample of dimensions 175 × 60 × 40 μm. The sample was loaded into a Merrill-Bassett-type diamond anvil cell

Received: November 27, 2012
Published: January 15, 2013

   dx.doi.org/10.1021/ja311613p | *J. Am. Chem. Soc.* 2013, 135, 1252−1255

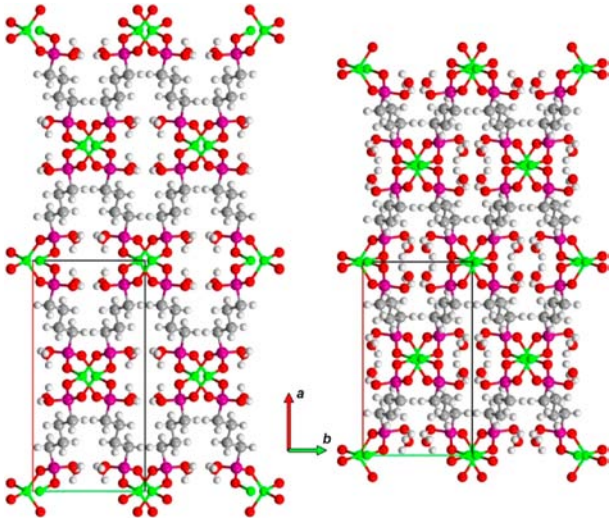

Figure 1. ZAG-4 as viewed down the *c*-axis for the ambient (left) and 7.32(7) GPa (right) structures.

(DAC) with Bohler-Almax cut diamonds, with culets of 600 μm in tungsten-carbide backing seats, and a tungsten gasket with hole diameter of 350 μm. The pressure medium used was a 4:1 methanol/ethanol mixture. The crystal was first affixed to the surface of the diamond culet using a silicon vacuum grease before the gasket was set in place. A small amount of ruby powder was added for pressure calibration and the methanol/ethanol added before closing the DAC. The cell was pressurized to 1.65 GPa initially and was allowed to stabilize for 3 h before data collection.

Data collection was performed at Beamline 11.3.1 at the Advanced Light Source (ALS) at Lawrence Berkeley National Lab (LBNL). In situ diffraction experiments were performed using synchrotron radiation (λ = 0.60480 Å) on a modified Bruker APEX-II diffractometer system. To maximize the data obtained, three data sets were run at each pressure with a rotation of the DAC by 120° resulting in three total data sets per pressure. Each data set included a series of phi and omega scans at 3 s per frame. The pressure of the cell was monitored between each data set for pressure stability and to make sure there was no methanol/ethanol leakage leading to pressure loss. The pressure was monitored via ruby fluorescence stimulated by a 100W 447 nm diode, measured via fiber-optic coupled to a Princeton Instruments Acton 300i spectrometer.[18] Data were collected at pressures of 1.65(10), 2.81(9), 5.69(3), and 7.32(7) GPa. The pressure within the DAC was raised to 9.9(2) GPa (as calculated from the ruby fluorescence measured); however, during data collection, the gasket failed under this pressure and the pressure fluid escaped until stabilizing at 5.0 GPa. The cell was then unloaded and the crystal was removed and cleaned under oil before being remounted on a MiTeGen kapton pin for data collection at room temperature.

ZAG-4 is considerably resilient under hydrostatic conditions, with respect to crystallinity. The framework continues to diffract with decreasing intensity, but with relatively little peak broadening. The volume decreases 27% over 7.3 GPa with the largest change of 11.5% occurring over the first 1.7 GPa of pressure. This is accompanied by an increase in density of 36%. The largest contributing factor to this change is the increase of the β angle from 113.837(2) to 123.227(8)°. All of the relative cell parameters with respect to the ambient parameters against applied pressure are shown in Figure 2. Figure 3 shows a plot of the change in volume with respect to pressure. From this curve,

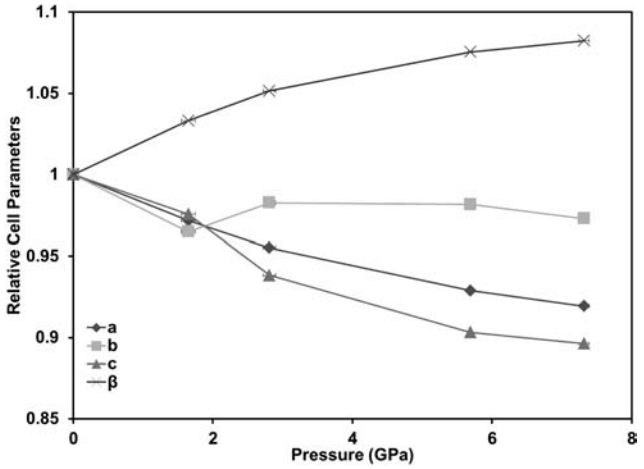

Figure 2. Experimental lattice parameter variation observed with respect to increase in pressure. Vertical error bars are contained within the markers.

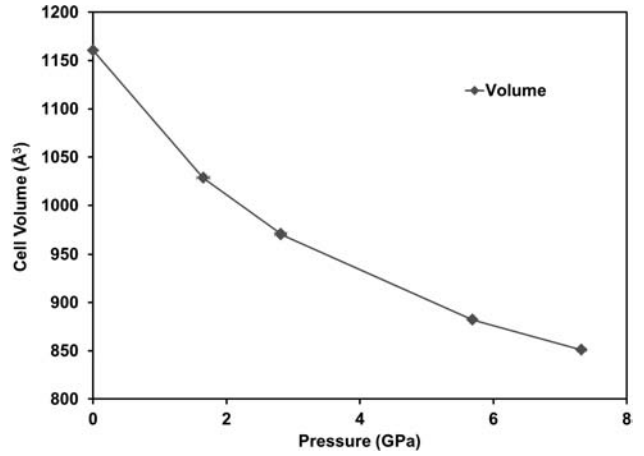

Figure 3. Experimental unit-cell volume variation observed with respect to increase in pressure. This is best fit by a fourth-order Birch–Murnaghan equation of state with K_0 = 11.66, K' = 1.976, and K'' = 1.3776. Vertical error bars are contained within the markers.

we can ascertain that the change in volume is best fit by a fourth-order Birch–Murnaghan equation of state; Table S1 shows the breakdown of the results of several equations of state calculations from the program eosfit.[19] Table S2 shows the packing index for each pressure.

Some of the largest changes in the structure are located in the inorganic 1-D chain. This is first observed by the greater than 10% decrease in the *c*-axis which contains this chain; however, inspection of the 8-membered chain-link provides a more complete explanation as shown in Figure 4. Figures 4A and 4B, which are representations of this 8-memembered ring at ambient pressure (A) and 7.32(7) GPa (B), clearly show that the distortion of the ring is due to an opening of the O1–Zn1–O2′ angle resulting in the Zn1–Zn1′ distance reducing from 4.245(1) to 3.754(1) Å. Figure 4C,D shows that the chair-type conformation of these rings is retained. While Figure 4 shows the localized deformation of a given link in the inorganic chain, Figure 5 shows that the long-range structure of the inorganic chain does not change substantially.

Further inspection of the inorganic chain shows that, from ambient to the applied pressure of 7.32(7) GPa, the chain actually expands in the *b*-axis direction a little over 0.2 Å. This is

dx.doi.org/10.1021/ja311613p | J. Am. Chem. Soc. 2013, 135, 1252–1255

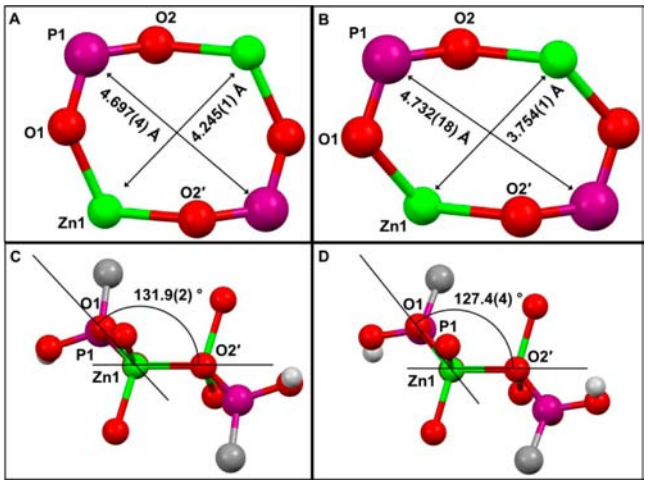

Figure 4. Representations of the 8-membered chain-link at ambient pressure (A, C) and 7.32(7) GPa (B, D) showing the ring (top) and the chair-like conformation (bottom). Solid black lines in the bottom represent calculated mean planes. The O1−Zn1−O2′ internal angle increases from 109.54(8) to 114.7(3)°. ′: $-x+1,-y+1,-z+2$.

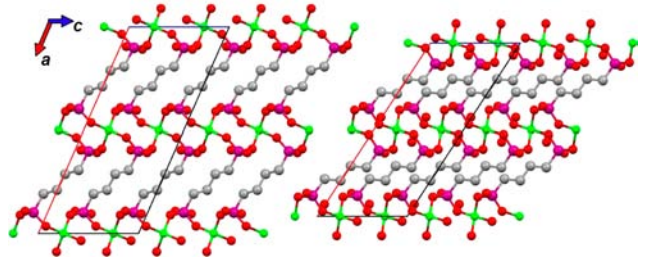

Figure 5. View down the *b*-axis of the ambient (left) and 7.32(7) GPa (right) structures.

quite substantial as it amounts to a change of approximately 2% on the *b*-axis. Initially, from ambient to 1.65(10) GPa, this chain compresses about 0.3 Å; on increasing to 2.81(9) GPa, the chain begins to expand nearly 0.1 Å and continues to expand through 7.32 GPa. These changes are best viewed in the movie files (Supporting Information (SI)).

One factor we have yet to explain is the changing linear compressibility of the *b*-axis. This direction lies perpendicular to the inorganic chains and contains all of the hydrogen bonding between the included water molecule and the free P−OH groups. Across the presented pressures, the shortest hydrogen bond (O3−H3···O1W) decreases from 2.557(3) to 2.37(2) Å. While the positions of the hydrogen atoms in these bonds are questionable, the interatomic distances are not. It is clear that the caged water molecules collapse inward to fill free space as best they can; however, the existence of the hydrogen atoms on the caged water molecules, as well as the hydroxide, reduces the amount of room available and limits the amount of compression. Following the aforementioned O3−H3···O1W distance, it is seen that the water molecules moves closer, shortening the distance from 2.557(3) to 2.460(9) Å initially, a change of 0.097 Å. Further pressure increases change this distance to 2.404(10), 2.406(10), and 2.37(2) Å, respectively. Taking into account the error on these values, there is compression from 1.65 to 2.81 GPa; however, the distance does not change with further applied pressure. This channel of hydrogen bonds combined with the expansion of the lateral direction of the inorganic chain explains why there is an initial decrease followed by an increase with a relative stand-still along the *b*-axis. Initially, this hydrogen bonded channel compresses, as does the inorganic chain, but then begins to push back strongly as the collective force of the hydrogen bonding strengthens, and the inorganic chain expands as well. We propose that it is the combination of these two structural features that causes the *b*-axis to compress and expand over the pressures presented.

This phenomena is not new; in 1998, Baughman et al. identified structures containing a "wine-rack" topology were among those predicted to exhibit negative linear compressibility.[20] While "wine-rack" describes the topology, "gate" does better to describe the mechanism. Cheetham et al. recently investigated this phenomenon in a zinc formate hybrid material, which they stated had been the first hybrid framework to the best of their knowledge reported showing negative linear compressibility.[21] In Cheetham's report, the negative linear compressibility results in an axis change of less than 1% over the applied pressure range of 0−1 GPa. Herein, we report that over the pressure range of 1.65−2.81 GPa, the negative linear compressibility results in a change of axis length of almost 2%

Table 1. Cell Parameters and Crystallographic Information for ZAG-4 at Different Pressures

pressure	ambient	1.65(10) GPa	2.81(9) GPa	5.69(3) GPa	7.32(7) GPa	ambient[a]
Space Group	*C*2/*c* (15)	*C*2/*c* (15)	*C*2/*c* (15)	*C*2/*c* (15)	*C*2/*c* (15)	*C*2/*c* (15)
Lambda (Å)	0.60480	0.60480	0.60480	0.60480	0.60480	0.60480
a (Å)	18.515(4)	17.991(2)	17.685(2)	17.1996(19)	17.023(2)	18.55(2)
b (Å)	8.291(2)	8.000(2)	8.147(2)	8.139(2)	8.066(3)	8.272(5)
c (Å)	8.265(2)	8.0643(6)	7.7557(6)	7.4651(6)	7.4078(8)	8.261(5)
β (deg)	113.837(2)	117.609(6)	119.697(6)	122.431(6)	123.227(8)	113.790(6)
V (Å^3)	1160.5(5)	1028.5(3)	970.6(3)	882.0(3)	850.9(3)	1160.1(13)
ρ (g/cm^3)	1.817	2.050	2.172	2.391	2.478	1.818
Reflections	1770	762	721	693	547	1713
Parameters	69	64	65	69	69	69
R_{int}	0.0453	0.0439	0.0537	0.0638	0.0630	0.0619
R_1/wR_2	0.0458/0.0960	0.0450/0.0963	0.0456/0.1125	0.0639/0.1369	0.0742/0.1580	0.0495/0.1137
θ Range	5.14−25.69	3.77−25.20	3.74−24.83	3.79−25.54	2.43−25.64	5.13−25.58

[a]Data taken on the single crystal which was removed from DAC after being brought to 9.9(2) GPa. All unit cells for data taken on pressurized samples are reported as unconventional representations utilizing the transformation matrix 1 0 2 0 −1 0 0 0 −1. This was done to maintain the same orientation as in the ambient structure.

dx.doi.org/10.1021/ja311613p | *J. Am. Chem. Soc.* 2013, 135, 1252−1255

(increasing from 8.000(2) to 8.147(2) Å). Furthermore, the axis decreases less than 0.5% over the next 3 GPa of applied pressure (8.147(2)−8.139(2) Å). As Cheetham and co-workers point out, this type of material is attractive for a variety of piezoresponsive applications such as pressure sensors, 'smart' body armor, pressure switches, and shock absorbing materials.[22,23] It is the inclusion of the caged water molecules in this compound that provides the unique axis compression character.

Despite the very large relative decreases in volume and the various cell parameters, after raising the pressure to 9.9 GPa and upon rapid removal of pressure, the process is completely reversible with all cell parameters returning to values within reasonable error of the ambient pressure room-temperature data. Table 1 shows the unit-cell parameters and crystal information for all pressures and the return to ambient pressure after the experiment. Of note, the quality of the crystal is maintained such that when the gasket failed at 9.9 GPa, during data collection, the expansion of the cell could be followed across the 3 h of data collection. Three movies in the SI animate the compression/expansion of the system across the pressures studied, as viewed down the *a*-, *b*-, and *c*-axis.

Taking everything into account, one can see how frameworks similar to the one presented herein may find their use as a new class of piezoelectric or piezomagnetic materials. By carefully studying the structural effects of pressure on these hybrid materials, one can begin to design new systems which may exhibit unique properties. It has been suggested that there are benefits to using hybrid materials over those that are either purely organic or inorganic.[9] They provide compounds that are often the best of both worlds. In the compound presented here, the alkyl chains provide a spring-like cushion to stabilize the compression of the system allowing for large distortions in the metal coordination environment, without destruction of the material.

We have demonstrated that the flexibility of an alkyl chain supported MOF can result in dramatic elastic behavior of a single crystal. ZAG-4 is highly compressible with reversibility possible within the regime of 10 GPa while maintaining single crystal quality. The axis orthogonal to the *bc*-plane exhibits remarkable compressibility of nearly 17%, while the inorganic chain direction also compresses over 10%. Despite these large compressions in the *a*- and *c*-axes, the *b*-axis exhibits both positive and negative linear compressibility. Further investigation is necessary to determine the upper bound of the reversible nature of this material. Future studies will include the systematic pressure study of the reticularly extended ZAG-6 compound, as well as nanoindentation experiments on both ZAG-4 and ZAG-6 to determine the mechanical properties of these materials. We hope through these studies to better understand the changing linear compressibility of the *b*-axis in ZAG-4 and whether it exists in ZAG-6 as well. Further, we may unveil that phosphonate MOFs and related compounds exhibit interesting piezoelectric and piezomagnetic properties while withstanding remarkable mechanical external forces, and may find applications in piezoresponsive materials.

■ ASSOCIATED CONTENT

Supporting Information

CIF files, synthesis information, tables containing the equation of state calculation results, rocking curves, full-size versions of the structural figures and movies depicting the compression of the framework as viewed along each axis. This material is available free of charge via the Internet at http://pubs.acs.org.

■ AUTHOR INFORMATION

Corresponding Author

kgagnon@mail.chem.tamu.edu.

Notes

The authors declare no competing financial interest.

■ ACKNOWLEDGMENTS

The authors thankfully acknowledge the National Science Foundation (Grant DMR-0652166) as well as the Robert A. Welch Foundation (Grant 10673). K.J.G. thanks the National Science Foundation for support through the NSF GRFP grant no. DGE-0750732. The Advanced Light Source is supported by the Director, Office of Science, Office of Basic Energy Sciences, of the U.S. Department of Energy under Contract No. DE-AC02-05CH11231.

■ REFERENCES

(1) Barthelet, K.; Marrot, J.; Riou, D.; Férey, G. *Ang. Chem. Int. Ed.* **2002**, *41* (2), 281.
(2) Yaghi, O. M.; O'Keeffe, M.; Ockwig, N. W.; Chae, H. K.; Eddaoudi, M.; Kim, J. *Nature* **2003**, *423* (6941), 705.
(3) Maeda, K. *Microporous Mesoporous Mater.* **2004**, *73* (1−2), 47.
(4) Rowsell, J. L. C.; Millward, A. R.; Park, K. S.; Yaghi, O. M. *J. Am. Chem. Soc.* **2004**, *126* (18), 5666.
(5) Special Issue on Metal-Organic Frameworks . *Chem. Rev.* **2012**, *112*, 673−1268.
(6) Shimizu, G. K. H.; Vaidhyanathan, R.; Taylor, J. M. *Chem. Soc. Rev.* **2009**, *38* (5), 1430.
(7) Aromí, G.; Barrios, L. A.; Roubeau, O.; Gamez, P. *Coord. Chem. Rev.* **2011**, *255* (5−6), 485.
(8) Phan, A.; Doonan, C. J.; Uribe-Romo, F. J.; Knobler, C. B.; O'Keeffe, M.; Yaghi, O. M. *Acc. Chem. Res.* **2009**, *43* (1), 58.
(9) Tan, J. C.; Cheetham, A. K. *Chem. Soc. Rev.* **2011**, *40* (2), 1059.
(10) Parise, J. B. *Rev. Mineral. Geochem.* **2006**, *63* (1), 205.
(11) Chapman, K. W.; Halder, G. J.; Chupas, P. J. *J. Am. Chem. Soc.* **2008**, *130* (32), 10524.
(12) Chapman, K. W.; Halder, G. J.; Chupas, P. J. *J. Am. Chem. Soc.* **2009**, *131* (48), 17546.
(13) Graham, A. J.; Allan, D. R.; Muszkiewicz, A.; Morrison, C. A.; Moggach, S. A. *Ang. Chem. Int. Ed.* **2011**, *50* (47), 11138.
(14) Ogborn, J. M.; Collings, I. E.; Moggach, S. A.; Thompson, A. L.; Goodwin, A. L. *Chem. Sci.* **2012**, *3* (10), 3011.
(15) Gagnon, K. J.; Perry, H. P.; Clearfield, A. *Chem. Rev.* **2011**, *112* (2), 1034.
(16) Arnold, D. I. The Synthesis and Characterization of Zinc(II) and Copper(II) Diphophonatoalkanes. Master's Thesis, Texas A&M University, 2000.
(17) Fu, R.-B.; Wu, X.-T.; Hu, S.-M.; Zhang, J.-J.; Fu, Z.-Y.; Du, W.-X. *Polyhedron* **2003**, *22* (19), 2739.
(18) Piermarini, G. J.; Block, S.; Barnett, J. D.; Forman, R. A. *J. App. Phys.* **1975**, *46* (6), 2774.
(19) Angel, R. J. *Rev. Mineral. Geochem.* **2000**, *41* (1), 35.
(20) Baughman, R. H.; Stafström, S.; Cui, C.; Dantas, S. O. *Science* **1998**, *279* (5356), 1522.
(21) Li, W.; Probert, M. R.; Kosa, M.; Bennett, T. D.; Thirumurugan, A.; Burwood, R. P.; Parinello, M.; Howard, J. A. K.; Cheetham, A. K. *J. Am. Chem. Soc.* **2012**, *134* (29), 11940.
(22) Godwin, J. G.; Ge, X.; Stephan, K.; Jurisch, A.; Tullius, S. G.; Iacomini, J. *Proc. Natl. Acad. Sci. U.S.A.* **2010**, *107* (32), 14339.
(23) Grima, J. N.; Attard, D.; Caruana-Gauci, R.; Gatt, R. *Scr. Mater.* **2011**, *65* (7), 565.